Analytical and Bioanalytical Chemistry
https://doi.org/10.1007/s00216-018-1106-7

RESEARCH PAPER

Mussel-inspired 3D fiber scaffolds for heart-on-a-chip toxicity studies of engineered nanomaterials

Seungkuk Ahn[1] · Herdeline Ann M. Ardoña[1] · Johan U. Lind[1,2] · Feyisayo Eweje[1] · Sean L. Kim[1] · Grant M. Gonzalez[1] · Qihan Liu[1] · John F. Zimmerman[1] · Georgios Pyrgiotakis[3] · Zhenyuan Zhang[3] · Juan Beltran-Huarac[3] · Paul Carpinone[3] · Brij M. Moudgil[3] · Philip Demokritou[3] · Kevin Kit Parker[1]

Received: 3 March 2018 / Revised: 10 April 2018 / Accepted: 23 April 2018

Abstract

Due to the unique physicochemical properties exhibited by materials with nanoscale dimensions, there is currently a continuous increase in the number of engineered nanomaterials (ENMs) used in consumer goods. However, several reports associate ENM exposure to negative health outcomes such as cardiovascular diseases. Therefore, understanding the pathological consequences of ENM exposure represents an important challenge, requiring model systems that can provide mechanistic insights across different levels of ENM-based toxicity. To achieve this, we developed a mussel-inspired 3D microphysiological system (MPS) to measure cardiac contractility in the presence of ENMs. While multiple cardiac MPS have been reported as alternatives to in vivo testing, most systems only partially recapitulate the native extracellular matrix (ECM) structure. Here, we show how adhesive and aligned polydopamine (PDA)/polycaprolactone (PCL) nanofiber can be used to emulate the 3D native ECM environment of the myocardium. Such nanofiber scaffolds can support the formation of anisotropic and contractile muscular tissues. By integrating these fibers in a cardiac MPS, we assessed the effects of TiO_2 and Ag nanoparticles on the contractile function of cardiac tissues. We found that these ENMs decrease the contractile function of cardiac tissues through structural damage to tissue architecture. Furthermore, the MPS with embedded sensors herein presents a way to non-invasively monitor the effects of ENM on cardiac tissue contractility at different time points. These results demonstrate the utility of our MPS as an analytical platform for understanding the functional impacts of ENMs while providing a biomimetic microenvironment to in vitro cardiac tissue samples.

Keywords Polydopamine · Nanofiber · Microphysiological systems · Cardiotoxicity · Nanotoxicology

Introduction

Engineered nanomaterials (ENMs) have unique size-dependent optical, magnetic, and electrical, properties, which can be difficult to achieve using their bulk counterparts. Consequently, the use of ENMs has greatly increased in consumer products, with applications in cosmetics, electronics, and even drug delivery. Because ENMs are often designed to be evenly distributed, insoluble, and stable, this makes them difficult to safely dispose [1] and therefore increases their potential to act as environmental pollutants. This, in turn, presents the risk of being exposed to ENMs via unintended routes, such as through ambient air inhalation or oral ingestion via ground and drinking water. As a result, understanding the pathological consequences of organ exposure to ENMs poses an important challenge that has not been fully explored [2, 3]. This is particularly alarming as some early reports have already linked ENM

Published in the topical collection *Analytical Developments in Advancing Safety in Nanotechnology* with guest editors Lisa Holland and Wenwan Zhong.

Electronic supplementary material The online version of this article (https://doi.org/10.1007/s00216-018-1106-7) contains supplementary material, which is available to authorized users.

✉ Kevin Kit Parker
kkparker@seas.harvard.edu

[1] Disease Biophysics Group, Wyss Institute for Biologically Inspired Engineering, John A. Paulson School of Engineering and Applied Sciences, Harvard University, 29 Oxford Street, Cambridge, MA 02138, USA

[2] Present address: Department of Micro- and Nanotechnology, Technical University of Denmark, 2800 Kongens Lyngby, Denmark

[3] Center for Nanotechnology and Nanotoxicology, Harvard T.H. Chan School of Public Health, Harvard University, Cambridge, MA 02138, USA

Published online: 10 May 2018

exposure with cardiac failure and, potentially, death [4]. For instance, exposure to TiO_2 nanoparticles, which are abundantly used in white pigments, sunscreens, and food colorants, leads to a dose-dependent increase of heart rate due to ENM-induced arrhythmia under ex vivo exposure conditions of guinea pig hearts [5]. Additionally, Ag nanoparticles, which are industrially used in mirrors and photography and as antimicrobial or conducting agents, have also been found to diminish action potential readings in mice and lead to loss in myocardial excitability that induces lethal bradyarrhythmia [6]. Collectively, this marks TiO_2 and Ag as particularly important targets, not only because of their deleterious role in cardiac health but also because of their widespread manufacture and distribution [7]. Although significant progress has been made in identifying the cellular impacts of multiple ENMs, more investigations are needed to fully understand their mechanism of action and disease pathophysiology. Among the limitations of expanding the nanotoxicological studies are the high cost, low throughput, and ethical concerns of experiments involving in vivo and ex vivo models [8]. Accordingly, there is a great need for developing in vitro systems with physiologically relevant architectures and high throughputs.

Cardiac microphysiological systems (MPSs) and heart-on-chips have been developed as in vitro platforms in an effort to study the cardiopathology and cardiotoxicity [9–14]. Muscular thin films (MTFs), consisting of 2D anisotropic muscle tissues, have been successfully used in disease modeling and drug screening in previous reports [9–19]. The microstructure of the MTF platforms, built by micromolding or microcontact printing methods, enables the construction of highly aligned and contractile laminar tissues. While MTFs replicate the essential anisotropic architecture of cardiac muscle to provide physiologically relevant functional outputs in vitro, it is still important to recapitulate the native 3D microenvironment. Recently, nanofiber has obtained a great deal of attention due to their similarity to the topographical features of natural extracellular matrix (ECM) networks [20–23]. To date, synthetic nanofiber scaffolds have shown promise as a means of developing in vitro tissue-engineered 3D cardiac models [21–23]. Nonetheless, creating MPS that integrate nanofiber as structural cues with functional readouts remains challenging. In particular, there is a need to improve the adhesion between fiber layers and device parts, while simultaneously ensuring cellular adhesion and the formation of functional tissues.

To address these challenges, we developed adhesive biohybrid nanofiber scaffolds that can mimic the native cardiac ECM and can adhere to a range of MPS designs. We implement the scaffolds in MPS to generate in vitro 3D cardiac tissue models for nanotoxicology studies, with facile readouts of tissue contractility. Inspired by the ability of mussels to adhere to wet and dry surfaces, we functionalized nanofiber scaffolds with chemical mimics of 3,4-dihydroxyphenylalanine (DOPA)—a post-translationally modified amino acid, which serves as the key adhesive component of mussel foot proteins [24, 25]. Recently, several groups have developed adhesive materials based on polydopamine (PDA), which has a similar chemical structure and function to DOPA [24]. PDA can be easily synthesized from dopamine (DA) via catechol oxidation chemistry at alkaline conditions [26], has been applied to diverse substrates (both 2D and 3D), and has been used as a substrate material for improved cell adhesion and tissue development [27–30]. In this study, highly aligned polycaprolactone (PCL) nanofiber doped with DA was spun using a pull spinning system with centrifugal shear force [23]. Subsequent to spinning, DA units incorporated within the fibers were polymerized at basic pH to generate PCL/PDA nanofiber [24, 29, 31–33], which can enhance protein coating, adhesion of cells, and attachment of fiber layers to the surface of MPS devices. Here, we demonstrated the ability of this nanofibrous scaffold to guide the formation of anisotropic and functional cardiac tissues. Finally, we investigated the effect of direct ENM exposures on cardiac tissues using fiber-coated microphysiological devices based on cantilever designs, similar to those in conventional MTF assays [9–14]. We observed that exposure to a high dose of TiO_2 and to Ag nanoparticles disrupted the structure and function of cardiac tissues in vitro. These studies explored the capability of our fiber-coated MPS as a platform for conducting physiologically relevant nanotoxicology studies of 3D cardiac tissues.

Materials and methods

Fiber fabrication and polymerization

Nanofibers were fabricated by using a pull spinning system (see Electronic Supplementary Material (ESM) Fig. S1) as described previously [23]. PCL (6% *w/v*; Sigma) and dopamine hydrochloride (1% *w/v*, DA; Sigma-Aldrich, MO, USA) were dissolved in hexafluoroisopropanol (HFIP; Oakwood Chemicals, SC, USA) and mixed overnight. The polymer solution was introduced to the reservoir at a flow rate of 0.2 mL/min. The rotating bristle comes in contact and elongates the polymer droplet at 30,000 RPM to form continuous fibers. The spun fibers were dried for 2 h in a chemical fume hood to remove excess HFIP before further characterization and measurement. After drying the fibers, they were incubated with triethylammonium bicarbonate (TEAB, pH 8.5; Sigma-Aldrich, MO, USA) buffer for about 20 h to initiate polymerization. After the reaction, the polymerized fibers were washed by ultrapure deionized water (Invitrogen, Thermo Fisher Scientific, MA, USA) at least three times.

Scanning electron microscopy

The fibers were prepared on scanning electron microscopy (SEM) stubs and sputter-coated with Pt/Pd (Denton Vacuum, NJ, USA) with a thickness of 5 nm. Field emission scanning electron microscopy (FESEM; Zeiss) was used to obtain SEM images of the fibers.

Analysis of fiber diameter and alignment

ImageJ software (NIH) with the DiameterJ plug-in was used to determine fiber diameter and alignment from the SEM images of the fibers as described in a previous study [34].

Fourier transform infrared spectroscopy

The Fourier transform infrared (FTIR) spectra of the fiber scaffolds were measured by using attenuated total reflectance-Fourier transform infrared spectroscopy (ATR-FTIR; Lumos, Bruker, MA, USA). As a control sample, PCL/PDA film was prepared by dropping and drying a solution of PCL (6% *w/v*) in HFIP doped with DA (0.2% *w/v*) in TEAB at room temperature. For each sample, the recorded spectrum was collected from a total of 16 scans and was then normalized from 0 to 1 by using OriginPro 8.6 software (Origin Lab Corporation).

Mechanical property testing

Mechanical uniaxial testing followed ASTM International standard C1557-14 to measure the modulus of fiber sheets. A polycarbonate sheet with a thickness of 150 μm (McMaster, NJ, USA) was cut into frames with a gauge length of 5 mm to match the length of the MPS cantilevers. Fiber samples were cut to 10 mm length and secured to the frame using epoxy (5 Minute; Devcon, MA, USA), which was cured for 24 h. After sample preparation, a frame with a sample was loaded into pneumatic grips of an Instron model 5566 equipped with a 10 N load cell. After loading, the frame was cut to allow for pulling of the sample only. For testing, 10 cycles of loading to 10% strain at 0.5, 1, 2, and 3 Hz was performed to match the loading condition of the cantilever. Since there was no significant difference between the measurements at different frequencies, modulus at 1 Hz was only reported in the main text. The specific modulus of each sample was calculated by dividing the modulus (MPa) by density (g/cm^3).

Qualitative adhesive property testing

To evaluate the bioadhesive property of the fiber scaffolds, we assessed the extent of fibronectin (FN; BD Biosciences, CA, USA) coating at the fiber surfaces. The spun fiber scaffolds were incubated with 50 μg/mL of FN solution in deionized water for 6 h at room temperature. After which, the samples were washed with deionized water three times and were then incubated with anti-FN antibody (rabbit; Abcam, MA, USA) and a secondary antibody (goat anti-rabbit IgG (H+L) conjugated with Alexa Fluor® 546, Invitrogen, Thermo Fisher Scientific, MA, USA) separately, for 1 h each. The micrographs of the fluorescently stained samples were obtained using a spinning disk confocal microscope (Olympus ix83, Andor spinning disk). The images were recorded on a Hamamatsu Orca Flash 4.0 C11440 at 16 bit depth with a 0.16- to 0.33-μm pixel resolution. For the statistical analysis of FN absorption on the nanofiber, the fluorescent FN images on the nanofiber were recorded for multiple samples ($n = 3$) with multiple regions of interest (ROIs, at least 25) for each condition. The coverage of FN on the nanofiber was calculated using ImageJ software and then normalized to the FN coverage on PCL/DA nanofiber using OriginPro 8.6 software.

Neonatal rat ventricular myocyte culture

All protocols for animal experiments done in this study were approved by the Institutional Animal Care and Use Committee (IACUC) at Harvard University. Neonatal rat ventricular myocytes (NRVMs) were isolated from 2-day-old Sprague Dawley rats by following previous protocols [9]. The NRVMs were cultured on the scaffolds with M199 culture media supplemented with 10% heat-inactivated fetal bovine serum (FBS), 10 mM HEPES, 0.1 mM MEM non-essential amino acids, 20 mM glucose, 2 mM L-glutamine, 1.5 μM vitamin B_{12}, and 50 U/mL penicillin. The FBS concentration was decreased to 2% after the first 48 h in culture. A kymograph of the contraction over time was generated using ImageJ software.

Immunostaining

The cells were fixed in 4% paraformaldehyde (PFA) and 0.05% Triton-X for 10 min. After fixation, the samples were incubated with a primary antibody against sarcomeric α-actinin (Sigma-Aldrich, MO, USA) and 4*n*,6-diamidino-2-phenylindole dihydrochloride (DAPI; Molecular Probes, Thermo Fisher Scientific, MA, USA) for 2 h at room temperature, followed by a secondary antibody against rabbit IgG (H+L) conjugated to Alexa Fluor® 546 (Invitrogen, Thermo Fisher Scientific, MA, USA) for 1 h at room temperature. The samples were washed by 1× phosphate-buffered saline (PBS; Gibco, Thermo Fisher Scientific, MA, USA) and were mounted on a glass slide with ProLong Gold antifade agent (Invitrogen, Thermo Fisher Scientific, MA, USA). Confocal microscopy (Zeiss LSM 7 LIVE) was used to obtain images of immunostained cells. Three-dimensional reconstruction of z-stacked images was performed using Zen lite 2.3 software (Zeiss).

Cytotoxicity measurement

A traditional lactate dehydrogenase (LDH) assay (Promega, WI, USA) was utilized to measure ENM-induced cytotoxicity for NRVMs cultured on PCL/PDA nanofiber-coated MPS as described previously [35, 36]. The cell culture media from each sample were collected in triplicate and then incubated with the reagents from the LDH assay kit. The absorbance of the resulting solution at 490 nm was recorded using a plate reader (Synergy HT, BioTek, VT, USA). Due to the considerable spectral overlap of the colorimetric components of the said LDH assay with the absorption of Ag nanoparticles, the assay was not performed for the samples exposed to Ag. The cytotoxic effect of Ag at the working concentration used for the experiments in this study (50 μg/mL) was also assessed using an MTT (3-(4,5-dimethylthiazol-2-yl)-2,5-diphenyltetrazolium bromide) assay kit (Thermo Fisher Scientific, MA, USA). The background absorption from Ag nanoparticles was subtracted accordingly.

Quantitative analysis of maturation of cardiomyocytes

The maturity of cardiomyocytes (sarcomere alignment, length, and packing density) on the scaffolds was evaluated by using algorithms in ImageJ and MATLAB (MathWorks) as previously described [37, 38]. In these algorithms, orientational order parameter (OOP) helps to quantify the sarcomeric z-line formation in cardiac tissues, scaling from 0 (no alignment) to 1 (perfect alignment) based on the degree of the uniaxial sarcomere components at a tissue level [37, 38]. Since the z-line registration plays a crucial role in contraction of cardiac tissues, OOP can be used to explain the contractile strength of the engineered cardiac tissues [37, 38].

Fabrication of nanofiber-coated MPS

Gelatin (Sigma-Aldrich, MO, USA) and microbial transglutaminase (MTG; Ajinomoto, NJ, USA) were prepared with deionized water as 10 and 4% *w/v* solutions, respectively. The gelatin solution was pre-warmed to 60 °C to homogenously dissolve all powder, followed by mixing with a pre-warmed MTG solution at 37 °C. To prepare the bottom substrates (see ESM Fig. S2), clean acrylic sheets (0.4 × 22 × 22 mm; Astra Products, NY, USA) were covered with a low-adhesive tape (3M, MN, USA) that was pre-patterned using a laser engraving system (30 W, 24 × 12; Epilog Laser Mini, CO, USA). A selected portion was peeled and exposed to plasma treatment for 2 min (SPI Plasma Prep II, PA, USA). After which, the adjacent untreated area was also peeled off. Upon mixing gelatin and MTG, the resulting solution was quickly pipetted onto the exposed area. A polydimethylsiloxane (PDMS) block and 200 g metal weight were sequentially placed on top of the gelatin-MTG drop to have a homogenous gelatin film thickness. After curing, the PDMS was carefully lifted off the gelatin surface. To these gelatin substrates, 3 mL of PCL/DA (6/1% *w/v*) solution in HFIP was spun (four chips per run). The fiber-coated devices were incubated with TEAB buffer for about 20 h at room temperature to polymerize the DA units incorporated in PCL fibers. Once polymerized, the devices were washed by deionized water for at least three times and dried in a chemical hood at room temperature. After drying the devices, each chip was engraved with the layout of the cantilevers using the Epilog laser cutter system (10% speed, 3% power, and 2000 Hz frequency). Each fiber-coated gelatin MPS chip is comprised of six cantilevers (2 mm × 4 mm). The samples were then rehydrated in PBS and sterilized overnight under UV light. For seeding each MPS chip with cells, 200 μL of cell suspension with a concentration of 5000 cells/μL was directly pipetted onto the fiber surface. After incubating the chip with cells at 37 °C for 30 min, when the cells are well adhered to the fibers, 3 mL of culture media was slowly added onto the well (surface area, 9 cm^2) where the MPS chip is contained.

Fabrication of nanofiber-coated instrumented MPS

Instrumented cardiac MPSs were fabricated as previously described with additional steps for the nanofiber layer application [14]. The devices were constructed layer-by-layer on 127.9 mm × 85.8 mm × 1.0 mm glass substrates. First, silver contact pads were made along the long edges of the devices by stencil printing AG-510 (Applied Ink Solutions, MA, USA) and then annealed at 190 °C for 30 min. Following this step, poly(*N*-isopropylacrylamide) (PNIPAAm) release layer islands (2% *w/v* in isopropanol) were made using a pressure-sensitive pen. Subsequently, PDMS (Sylgard 184 Dow Corning, MI, USA) was applied by spin coating at 4000 RPM for 5 min, forming a 5.2-μm-thick layer. Following curing overnight at 65 °C, Ti-Au strain gauge wires were deposited in a two-step process using two stainless steel shadow masks (Newcut, NY, USA) and an e-beam evaporator (Denton, NJ, USA). A second layer of PDMS was added by spin coating at 2000 RPM for 5 min, equivalent to an 11.9-μm-thick layer. After curing, the devices were annealed to relieve residual stress in the wires by heating at 190 °C for 30 min.

The nanofiber layer was applied using pull spinning as described in previous sections. Prior to spinning fibers, the PDMS surface of the devices was incubated with (3-aminopropyl)triethoxysilane (APTES; Sigma-Aldrich, MO, USA) overnight in an evacuated desiccator. The devices were subjected to treatment with UV-ozone for 8 min preceding the APTES treatment to improve aminosilane adhesion to the PDMS substrate. The devices were rotated to collect fibers during spinning through attachment to a milled frame

connected to a DeWALT DC 720 0.5-in. cordless drill driver. Ten milliliters of the fiber solution was loaded into a plastic syringe (Becton Dickinson, NJ, USA) and flowed through polyfluoroalkoxy alkane tubing (Saint-Gobain, PA, USA) to a wide-point plastic needle at 0.2 mL/min by using an automated syringe pump (Harvard Apparatus, MA, USA). The bristle was rotated at 30,000 RPM while the solution was ejected, and the resulting fibers were collected on the device. After collection was complete, the nanofiber-coated devices were incubated with TEAB buffer for polymerization.

Cantilevers were cut from the device using the laser cutting system described above. To remove the fibers from areas of the substrate other than the cantilevers, the laser cutter was used to cut circular patterns around each cantilever at the lowest possible power to avoid damage to the strain gauge wires. A mask with the same pattern was cut from a sheet of low-adhesive tape (3M, MN, USA), which was pressed onto the substrate and then carefully removed. This removal process was repeated three times to ensure that the PDMS underneath the excess fibers was completely exposed for well plate attachment. Finally, milled polycarbonate wells were attached to the device by forming a thin PDMS gasket on the bottom of the well plate and joining it with the now PDMS substrate using O_2 plasma treatment.

ENM synthesis and physicochemical and morphological characterization

Citrate capped silver nanoparticles

The Ag nanoparticles were synthesized using a hydrothermal method. In this method, silver salts (silver nitrate) were reduced to metallic silver particles using sodium citrate at elevated temperatures [39, 40]. In a round-bottom flask containing a 0.25 mM $AgNO_3$ solution, a sodium citrate solution (0.25 mM) was added slowly with a syringe. The solution temperature was adjusted to 100 °C and the reaction carried on until no more H_2 was released. The suspension was then cooled and stored. The particles were characterized in terms of size, shape, purity, surface chemistry, endotoxins, and biological contaminants according to the protocols described by Beltran-Huarac et al. [41]. The results are summarized in the ESM (see Tables S1–S3 and Fig. S3).

Titania: commercially available TiO_2 Aeroxide P25 Degussa

The particles were characterized in terms of size, shape, crystallinity, density, surface area, porosity, purity, surface chemistry, endotoxins, and biological contaminants according to the protocols described by Beltran-Huarac et al. [41]. The results are summarized in the ESM (see ESM S1–S3, Figs. S4 and S5).

ENM dispersion preparation

The dispersion preparation, colloidal characterization, and dosimetric analysis were performed as described in great detail by DeLoid et al. [42–44]. The cup horn sonicator (Branson Sonifier S-450D, 400 W, with Branson 3-in. cup horn) was calibrated according to the protocol by Taurozzi et al. [45] and found to deliver 2.59 W/mL. A stock solution of ENMs in DNase/RNase-free distilled water (Invitrogen) was prepared at a concentration of 0.5 mg/mL and was used to determine the critical delivered sonication energy (DSE_{cr}). One milliliter of the stock solution was used to measure the hydrodynamical diameter (dH) with DLS (Malvern Nanosizer, Worcestershire, UK). The solution was sonicated for 1 min, vortexed for 30 s, and measured again. The process continued until the dH and polydispersity index (PDI) were not changing significantly (± 5%). The DSE_{cr} of an ENM is defined as the DSE (in J/mL) required to achieve a solution with the lowest particle agglomeration state in DI H_2O and is ENM-specific. All stock suspensions from that point on were prepared according to the DSE_{cr} and were then adjusted to the desired concentration. The DSE_{cr} for the TiO_2 suspensions was 380 J/mL. The 10 and 100 μg/mL TiO_2 working solutions used in ENM exposure experiments were prepared by diluting the 500 μg/mL stock solutions with NRVM culture medium. After 3 days of cardiac MTFs in culture, the samples were exposed to a specific TiO_2 dispersion concentration for 48 h before performing the optical measurements for MPS chips or devices. As our positive control for an ENM with known cytotoxic effects, citrated Ag nanoparticle colloidal suspensions in cell culture media were also prepared.

Optical measurements and analysis for nanofiber-coated MPS

At the time point of recording, each MPS sample was transferred onto a 35-mm Petri dish with a pre-warmed Tyrode's solution (1.8 mM $CaCl_2$, 5 mM glucose, 5 mM HEPES, 1 mM $MgCl_2$, 5.4 mM KCl, 135 mM NaCl, 0.33 mM NaH_2PO_4 at pH 7.4). The sample was washed with Tyrode's solution for at least three more times after the transfer to remove any free-floating nanoparticles and their aggregates. The cantilevers were carefully peeled off the acrylic sheet while the dish is on a heating block (37 °C) under a Leica MZ9.5 stereomicroscope (Wetzlar, Germany) with × 1.25 magnification. The macroscopic motions of the cantilever, such as bending or tissue contraction, were optically recorded for each chip for at least 5 s at 30 frames per s using a Basler A601f-2 camera (Exton, PA, USA), under spontaneous or paced conditions. The pacing was executed at 1, 2, and 3 Hz at 10 V using a MyoPacer cell stimulator (IonOptix, MA, USA). The changes in tissue contractile stresses upon ENM exposure were determined in correspondence with our previous work on MTF cantilevers. Previously, we have demonstrated that the

contractile stress of soft tissues on cantilever supports can be obtained by tracking the x-projection using a cantilever's edge to calculate curvature and using a modified Stoney's equation to obtain stress [11, 12, 15]. Similar to these previous reports, we assumed that the radius of curvature (R_{curv}) upon cantilever bending should be directly proportional to the contractile stress of the seeded cardiomyocyte layer (σ_{tissue}) [11, 12]. From the generated $1/R_{curv}$ plot over time from the optical recordings, we compared the extracted values proportional to σ_{tissue} across different ENM exposure conditions and performed statistical analysis. All ENMs were added in the culture media at day 3, which is 24 h after the cells are supplemented by a 2% FBS culture medium. Samples that showed no contraction prior to the addition of ENMs, assumed to be from poor tissue maturation, were excluded from the study. Spontaneous and stimulated contractions were then recorded on day 5, for both controls and samples containing ENMs. For the samples that did not show contractions at day 5 (48 h after ENM exposure), the x-projection at all recorded frames is equal to the maximum length of the cantilever, therefore yielding a value of 0 for the $1/R_{curv}$ as the calculated R_{curv} converges to infinity.

Data acquisition from nanofiber-coated instrumented MPS

Data was acquired using a custom polycarbonate connector and a Keithley Multichannel DMM 3706a. The two-wire resistance recordings were collected at a sampling rate of 60 Hz. A mechanical model based on a modified Stoney's equation was applied to convert to resistance readout to approximate the contractile stresses generated by the tissues, as previously described [14]. Custom MATLAB (MathWorks) scripts were used for quantifying relative resistance changes and converting to stress. For electrically paced samples, a median filter (5) was applied.

Calcium imaging

The calcium transients of cardiomyocyte samples were measured using a calcium-sensitive dye as described previously [46]. Fifty micrograms of Fluo-4 AM dye (Thermo Fisher Scientific, MA, USA) was prepared in Pluronic F-127 solution (20% in dimethyl sulfoxide, DMSO) at 37 °C. From this stock solution, 2 μL of the dye in DMSO was added to 2 mL of NRVM cell culture media with 2% FBS in 37 °C, where cardiomyocytes were incubated for 30 min. After incubation, the samples were washed with fresh 2% FBS media for 15 min. Then, the samples were moved to a 35-mm Petri dish with 4 mL of pre-warmed Tyrode's solution in 37 °C for imaging. Confocal microscopy (Zeiss LSM 7 LIVE) was used to obtain time-series images of the dye from the samples.

Statistical analysis

All data are shown as mean ± standard error of mean (SEM). One-way analysis of variance (ANOVA) was utilized to determine statistical significance (*$p < 0.10$ or **$p < 0.05$).

Results and Discussion

Fabrication and characterization of mussel-inspired adhesive nanofiber

Mussel-inspired adhesive nanofiber was produced by spinning precursor nanofiber and polymerizing the spun nanofiber via catechol oxidation chemistry occurring under alkaline conditions (Fig. 1a). The precursor nanofiber was fabricated by co-spinning PCL and DA in HFIP using a pull spinning system (Fig. 1b; see ESM Fig. S1) [23]. Due to the low molecular weight of DA, PCL was used as a carrier polymer to form hybrid nanofiber under shear forces generated in the system. Following previous reports [24, 29, 31–33, 47], the spun PCL/DA nanofiber was polymerized by incubating them in TEAB buffer whose pH (8.5) triggers oxidization and polymerization of the accessible monomer DA units incorporated in the PCL fibers (Fig. 1c). Although the structure of PDA remains poorly explored [47], herein, we used the term PDA as defined in the references. We chose to co-spin PCL and DA and do post-polymerization instead of surface coating PCL fibers with PDA, because the latter surface treatment causes non-homogeneous coating and potentially alters the nanofiber morphology [29, 48]. After initiating the polymerization, a color change was observed from white (PCL/DA) to deep brown (PCL/PDA) fibers (insets in Fig. 1b, c), which is consistent with previously reported PDA substrates [24, 31–33]. Fiber diameters of precursor and polymerized nanofiber were 579 ± 123 and 591 ± 143 nm (Fig. 1d), respectively, showing no significant difference in the fiber diameter before and after polymerization. Fiber alignment analysis (Fig. 1e) indicated that PCL/DA and PCL/PDA nanofibers were highly aligned because of circumferentially directed forces during fiber formation as previously described [23].

Beyond the observed color change in Fig. 1b, c, FT-IR spectra of the nanofiber were recorded to confirm the presence of newly formed bonds after the TEAB buffer treatment and to validate the occurrence of polymerization (Fig. 2a). The emergence of new IR bands near 1596 cm^{-1} (for C=C) and near 3200 cm^{-1} (for secondary amines, N–H) [49], after the alkaline treatment of PCL/DA nanofiber, is indicative that DA cyclization has occurred to form PDA units (Fig. 1a). It should nonetheless be noted that we did not quantify the extent of DA polymerization and the amount of PDA that remain integrated within the fiber construct after the reaction. We also investigated the mechanical strength of the nanofiber scaffolds as this

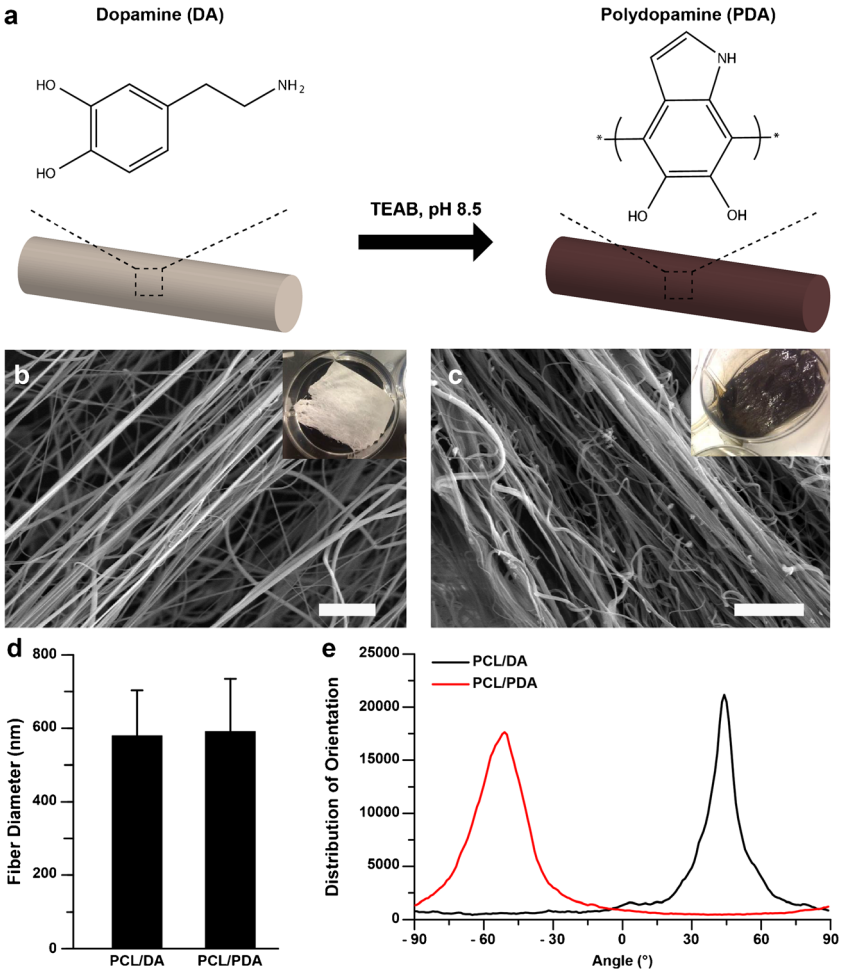

Fig. 1 Nanofiber fabrication. (**a**) Schematic illustration of polymerization of PCL/DA into PCL/PDA through treatment with triethylammonium bicarbonate (TEAB, pH 8.5) buffer. SEM images of (**b**) PCL/DA and (**c**) PCL/PDA. Insets indicate macroscopic images of nanofibers. Scales are 10 μm. (**d**) Fiber diameter analysis. $n = 4$. (**e**) Fiber directionality calculated from (**b**, **c**) SEM images

plays a crucial role in the optimal functionality of these fibers as tissue scaffolds. The specific modulus of PCL/DA and PCL/PDA nanofiber scaffolds was calculated as 98.0 ± 38.5 and 81.4 ± 16.7 MPa/(g/cm^3), respectively (Fig. 2b). There was no significant difference in the specific modulus before and after polymerization, which suggests that the TEAB treatment mostly yielded surface polymerization of DA to PDA. To assess the adhesive properties of the nanofiber, we evaluated the adhesion of an ECM protein (FN) by immunostaining (Fig. 2c–h). Fibronectin is one of the primary ECM proteins that control cell adhesion, proliferation, and functional tissue formation. After 6 h of incubation at room temperature, FN coverage on the surface of PCL/PDA nanofiber was higher than that on the surface of PCL/DA nanofiber (Fig. 2i). This observation is in line with previous studies showing higher protein and cell adhesion on PDA-coated PCL nanofiber compared to PCL nanofiber [28, 48].

In vitro cardiomyocyte culture on nanofiber

We hypothesized that the ECM-mimetic and adhesive properties of the nanofiber scaffold will support cardiomyocyte adhesion and functional tissue formation. To test the hypothesis, we cultured NRVMs on the scaffold. After a week of cell culture, contractile tissues were developed on the fibrous scaffold (Fig. 3a–c; see ESM Fig. S6). Kymograph of the contraction (Fig. 3d; see ESM Movie 1) reflects the regular and spontaneous beating of cardiomyocytes on the scaffold at a physiological range [50].

In an effort to further study the maturity of cardiomyocytes, we performed immunostaining for sarcomeric α-actinin and analyzed parameters related to sarcomere structure [37, 38]. First, the OOP is a metric to evaluate anisotropy of elements, where 0 and 1 mean no alignment and perfect alignment, respectively [37, 38]. From the cardiomyocytes seeded on our scaffolds, we observed anisotropic tissue formation along the long axis of the fiber direction (Fig. 3e). The sarcomeric OOP value for these cardiomyocytes grown on the mussel-inspired fiber scaffolds was 0.78 ± 0.04, showing very high tissue anisotropy. We also quantified the sarcomere length (SL) and sarcomere packing density (SPD) for our tissue samples to account for the existence of fully formed sarcomeres. The cardiac tissues on the scaffold exhibited 1.91 ± 0.08 μm (for SL) and 0.18 ± 0.09 (for SPD). The OOP, SL, and SPD

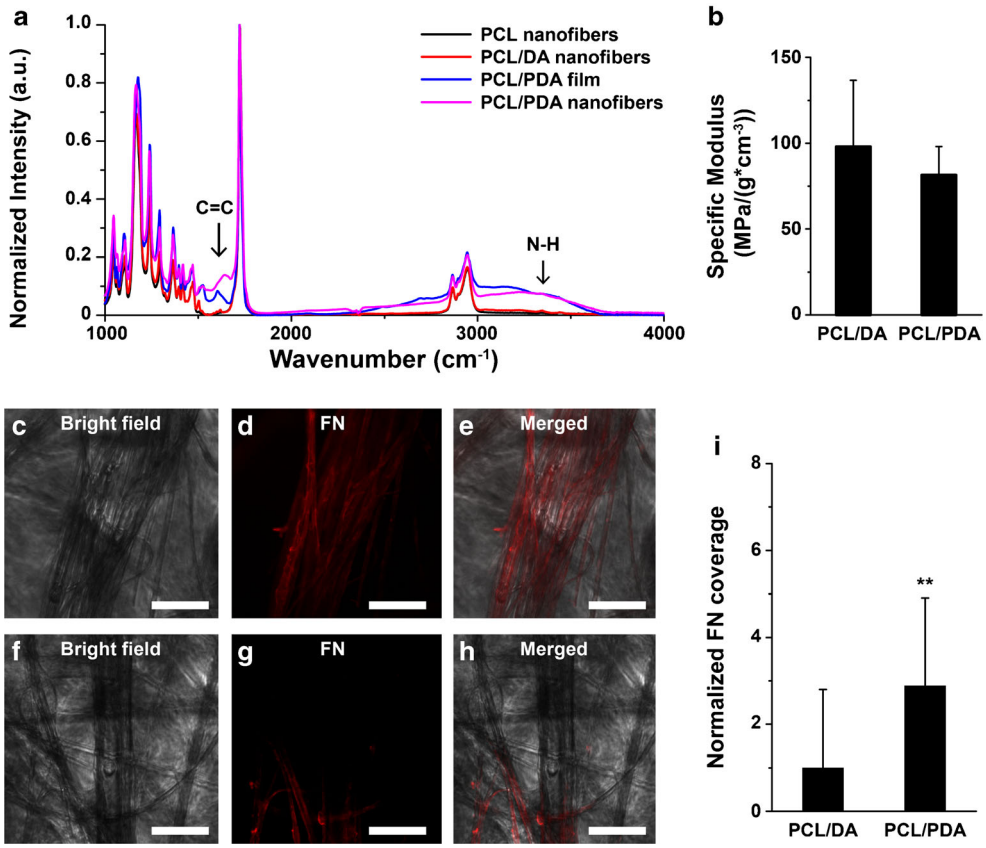

Fig. 2 Physicochemical properties of nanofiber. (**a**) FT-IR spectrum of PCL nanofiber, PCL/DA nanofiber, PCL/PDA film, and PCL/PDA nanofiber. (**b**) Specific modulus of nanofiber scaffolds. $n = 4$ for PCL/DA and $n = 5$ for PCL/PDA. (**c**–**i**) Adhesion of fibronectin on (**c**–**e**) PCL/PDA and (**f**–**h**) PCL/DA nanofiber. Scales are 100 μm. (**i**) FN coverages on the nanofiber were calculated and plotted. $^{**}p < 0.05$, $n = 3$, ROI of at least 25 for each condition

values from the tissues on PCL/PDA nanofiber were similar to those previously reported [37, 38] from the anisotropic and contractile tissues grown on 2D micropatterned substrates. Consequently, these data support our hypothesis that PCL/PDA nanofiber promotes 3D functional cardiac tissue formation (see ESM Fig. S6).

Fiber-coated cardiac microphysiological devices for nanotoxicology studies

To obtain functional data of contractile performance of the cardiac tissues, we integrated the mussel-inspired nanofiber scaffolds into an MPS design based on gelatin cantilever substrates

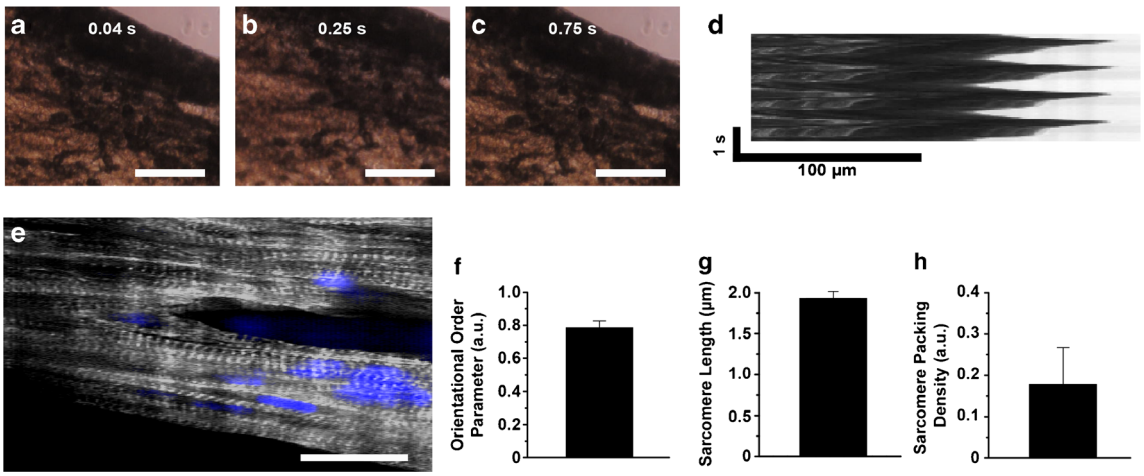

Fig. 3 In vitro cardiomyocyte culture on nanofiber. (**a**–**d**) Bright-field images of contraction of the fiber scaffolds with (**d**) kymograph. Scales of (**a**–**c**) are 100 μm. (**e**) Confocal image of cardiomyocytes on nanofiber, stained for nuclei (blue) and α-actinin (gray). Scale is 20 μm. (**f**) Orientational order parameter (OOP). (**g**) Sarcomere length. (**h**) Sarcomere packing density (SPD) of cardiomyocytes grown on the fibrous scaffolds. $n = 3$ and ROI = 4

[12]. By tracking the deflection of the cantilevers, we obtained in vitro readouts of contractile function of engineered cardiac tissues cultured in physiologically relevant 3D environments (Fig. 4a; see ESM Fig. S6 and Movie 2). We used $1/R_{curv}$ (Fig. 4b), which is directly proportional to the tissue contractile stress (σ_{tissue}), as a geometrical metric to assess the toxic effects of ENM exposure to cardiac tissues. This parameter is independent of any assumptions regarding the multilayer nature of the substrate. We therefore performed our nanotoxicological studies by comparing quantifiable geometric changes (i.e., $1/R_{curv}$) in the cantilever pre- and post-ENM exposure. By plotting $1/R_{curv}$ over time, we were able to extrapolate an analytical metric from the optical recordings that reflects the systolic and diastolic phases of contraction of the cardiomyocyte tissue layer (Fig. 4c, d). With the assumption that $1/R_{curv}$ is directly proportional to contractile tissue stress (σ_{tissue}) [11, 12, 15], normalizing the peak-to-peak amplitude of the $1/R_{curv}$ plots with respect to the measurements for the control samples (i.e., no ENM exposure) on the same day enables a relative comparison of the twitch stress across the cardiac MPS samples under different exposure conditions.

With the considerations for analysis discussed above, we assessed the tissue-level effects of ENM exposure at a low (10 μg/mL) and high (100 μg/mL) TiO_2 dose for NRVM tissues cultured on fiber-coated gelatin MPS samples. These concentrations were selected based on the range used in literature precedents that report cellular-level effects of TiO_2 to cardiac cells. A previous report on the cellular toxicity of TiO_2 nanoparticles on human embryonic stem cell-derived cardiomyocytes showed that 10 μg/mL TiO_2 has no significant cytotoxic effects, while a reduction in contraction amplitude was observed at 100 μg/mL [51]. This dose-dependent decrease in cell survival, as well as increase in reactive oxygen species (ROS) production, was also observed for rat cardiac (H9c2) cells directly exposed to 5 to 100 μg/mL of TiO_2 P25 Degussa nanoparticles [52]. Moreover, a typical nanoparticle used as a therapeutic drug transporter would be delivered at a concentration of 50 μg/20 g body weight, corresponding to 37 μg/mL [51, 53]. This concentration is within the range of test concentrations used in these studies (10–100 μg/mL).

The mechanism of action of TiO_2 toxicity is limited to general cellular-level information such as ROS generation, DNA peroxidation, or directly binding to LDH [54–56]. In rats, TiO_2 nanoparticles are reported to acutely alter cardiac excitability leading to arrhythmogenesis [57]. In a zebrafish model, chronic TiO_2 exposure resulted in alterations in cardiac muscle fibers, tissue-level inflammation and cell necrosis [58]. While the exact mechanisms of the cardiotoxic effects of TiO_2 on mammalian species are less understood, silver nanoparticles are well known to induce cytotoxic effects by enhancing ROS

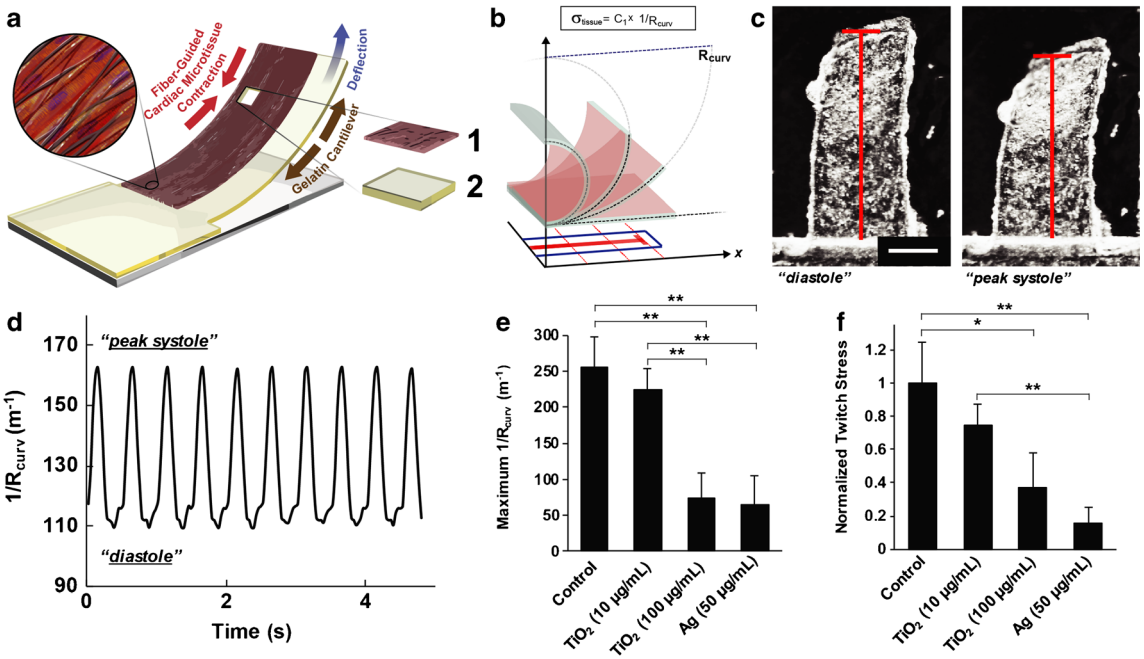

Fig. 4 Measuring contractile stress using fiber-coated gelatin MPS. (**a**) Principle sketch of a fiber-coated MPS with cardiomyocytes. Constituent layer 1, engineered cardiac tissue within nanofiber scaffolds; 2, gelatin thin film; see ESM Movie 2 for a representative video of a fiber-coated gelatin MPS seeded with contracting NRVMs. (**b**) Schematic diagram showing the extrapolation of x-projections of cantilever deflection in 2D and its correlation to R_{curv}. (**c**) Optical images showing the cantilever motions associated to cardiomyocyte diastole and systole. Scale is 1 mm. (**d**) Representative plot of the geometric readout from the optical recording of MPS motion over time, under 2 Hz pacing. Comparison of (**e**) maximum $1/R_{curv}$ and (**f**) normalized twitch stress values calculated from day 5 cardiac MPS samples under different ENM exposure conditions (48 h after ENM addition, 2 Hz pacing at 10 V). For statistical comparison, $*p < 0.10$ and $**p < 0.05$, $n = 10$ for control, $n = 6$ for 10 and 100 μg/mL and TiO_2, and $n = 7$ for Ag (50 μg/mL)

generation that leads to oxidative stress and inflammatory effects [59, 60]. Hence, we used Ag nanoparticles as a positive control ENM with pronounced cardiotoxicity.

We evaluated the effect of Ag and TiO_2 ENM on the contractile stress generated by the cardiac tissues on fiber-coated MPS, both spontaneously and under electrical pacing. In both cases, we observed a dose-dependent response where the samples exposed to 100 μg/mL concentration of TiO_2 showed lower contractile stresses than those exposed to 10 μg/mL and unexposed conditions (Fig. 4e, f). As a comparison, the observed maximum $1/R_{curv}$ and normalized twitch stress for samples with high-dose TiO_2 exposure were still higher than those exposed to the known cytotoxic Ag nanoparticles. For each condition (see ESM Table S4), we also calculated for the percentage of cantilevers beating at the time point of optical recording. Among the cantilevers exposed to 100 μg/mL TiO_2 and 50 μg/mL Ag, only 56 and 29% remained beating, respectively. For the other two conditions, 95% of the unexposed control and 92% of the 10 μg/mL TiO_2-exposed cantilevers remained beating across all the MPS samples at the time point of optical measurements. These results further support the observable impairment in contractile function due to the exposure of cardiac tissue samples to 100 μg/mL TiO_2 and 50 μg/mL Ag for 48 h.

Considering that our PDA-functionalized nanofibrous scaffolds potentially bind well to a range of materials, we took advantage of this adhesive property to integrate the fiber-supported cardiac tissues into instrumented MPS devices based on PDMS cantilevers with embedded flexible electronic contractility sensors (Fig. 5a; see ESM Movie 3). We recently reported this concept using MTFs developed on molded PDMS surfaces as cardiac tissue models [13, 14]. Furthermore, we previously demonstrated potential applications of the sensors for higher-throughput drug screening and time-resolved studies [13, 14]. Here, we show that it is straightforward to replace the molded PDMS surfaces with nanofibrous scaffolds, by coating the surface of the device with adhesive PCL/PDA nanofiber (Fig. 5a). This fiber-coated version combines a physiologically relevant 3D tissue microenvironment, with embedded sensors for non-invasive monitoring of tissue contractile stress. Taking advantage of the embedded sensors, we performed a proof-of-principle toxicity study of 100 μg/mL TiO_2 nanoparticles, monitoring contractile stress at multiple time points for the same cantilever. Again, we observed a relative decrease in the measurable twitch stress from spontaneously contracting cardiac microtissues after 48 h of exposure to 100 μg/mL TiO_2 as compared to the time point prior to ENM exposure (Fig. 5b). Additionally, we performed a proof-of-principle time-resolved study of tissue response to 100 μg/mL TiO_2, using the integrated electrical sensors. This indicated that the spontaneous contractions became negligible after merely 24 h of exposure (Fig. 5c).

To confirm the findings from our MPS-based studies on the influence of ENMs on cardiac tissue contractile function, we performed a colorimetric assay for LDH, a marker for tissue

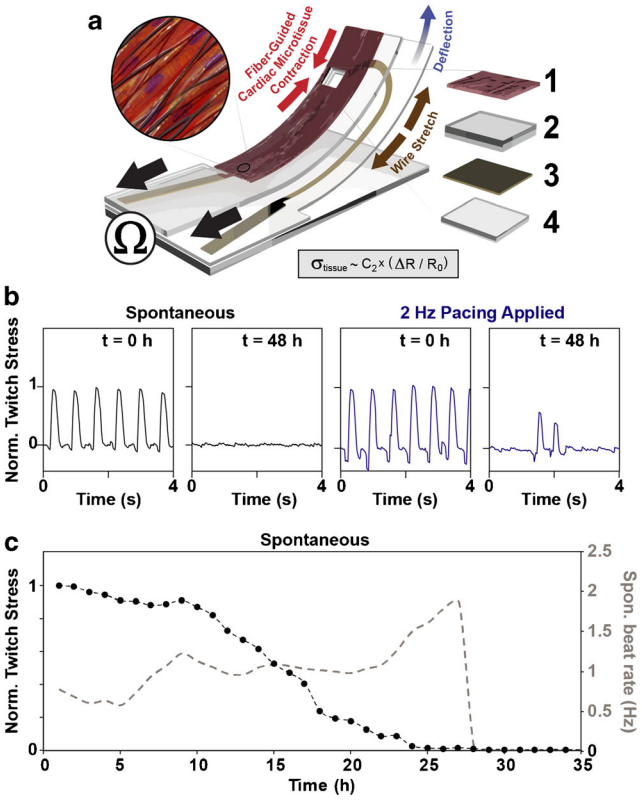

Fig. 5 Fiber-coated cardiac microphysiological device with embedded contractility sensors. (**a**) Principle sketch of device: an embedded flexible thin film sensor provides non-invasive electrical readout of contractile stress generated by PCL/PDA nanofiber-supported cardiac microtissue. Device adapted from Ref. [14] by introducing PCL/PDA nanofiber coating onto device surface. Constituent layer 1, engineered cardiac tissue within nanofiber scaffolds; 2, PDMS layer; 3, thin film sensor layer; 4, bottom PDMS layer; see ESM Movie 3 for a representative video of a fiber-coated device seeded with contracting NRVMs. (**b**) Electrical readout of normalized twitch stress generated by tissue prior to and after 48 h of exposure to 100 μg/mL TiO_2. (**c**) Electrical readout of normalized twitch stress (black traces, left axis) and beat rate (mean (3) gray trace, right axis) generated spontaneously by tissue during first 35 h of exposure to 100 μg/mL TiO_2

necrosis [61]. This allowed us to assess the impact of ENM exposure at the cellular level. Our results showed increased LDH levels upon exposure to 100 μg/mL TiO_2 as compared to the control and 10 μg/mL TiO_2 exposure (see ESM Fig. S7a). We also validated the cytotoxic effect of the Ag nanoparticle dose (50 μg/mL) used in these studies using an MTT assay (see ESM Fig. S7b) [62], whereby 48 h of NRVM exposure to Ag led to an 86% decrease in cellular viability.

We also investigated the electrophysiological effect of the nanoparticles using a calcium-sensitive dye (Fig. 6a–f) [46]. The fluorescent intensity of the dye during spontaneous contraction of cardiomyocytes was recorded using confocal microscopy and plotted. Calcium imaging showed that cardiomyocytes in the control sample contracted synchronously (Fig. 6a, b; see ESM Movie 4). After directly exposing the cardiac tissues in MPS samples to 10 μg/mL TiO_2 (Fig. 6c, d; see EMS Movie 5),

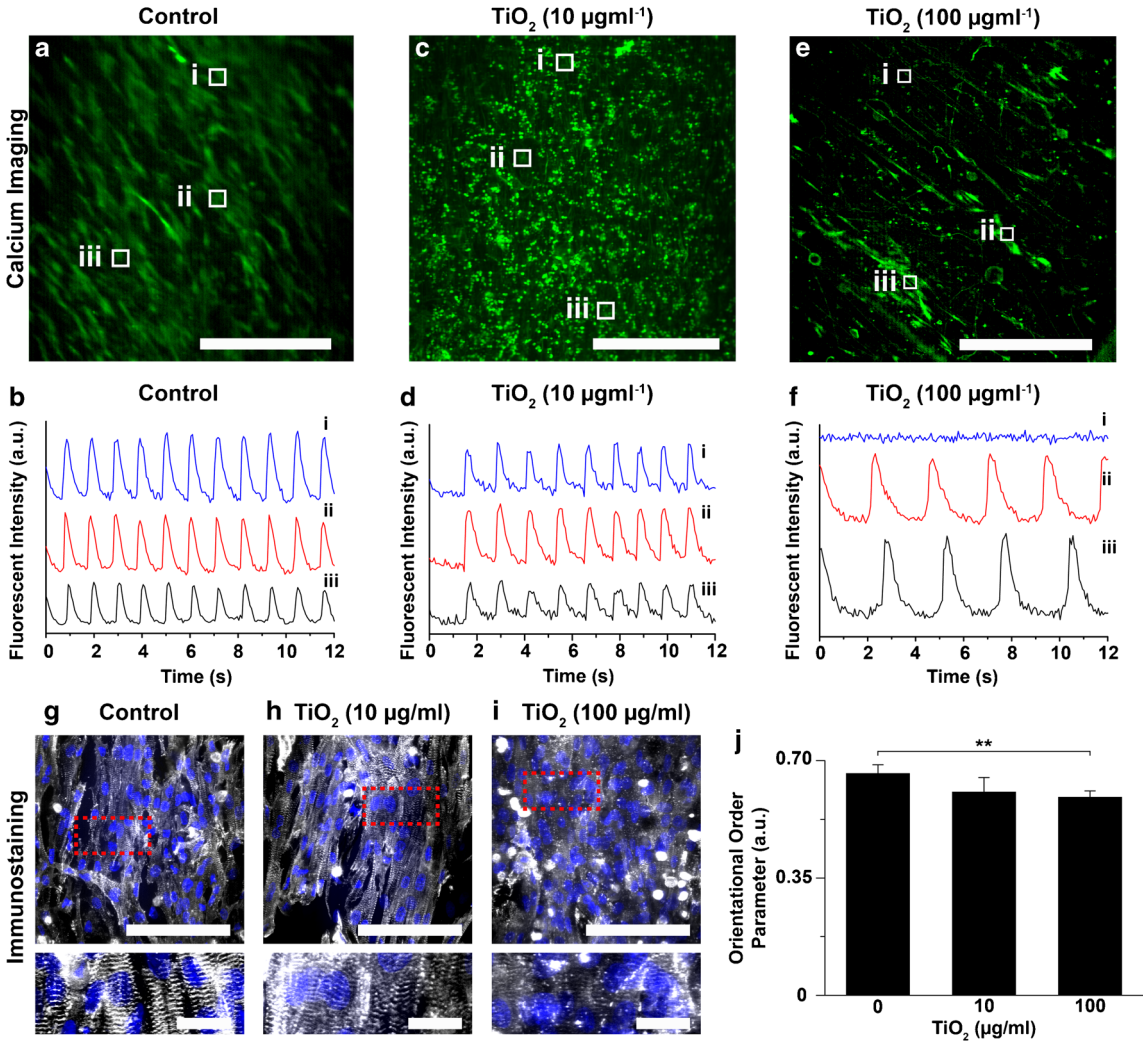

Fig. 6 Effect of ENMs on calcium transient and sarcomere structure. (**a**–**h**) Confocal images of calcium dye fluorescent (green) with calcium transient at the specific points (white boxes) for (**a**, **b**) control, (**c**, **d**) TiO_2 (10 μg/mL) exposure, and (**e**, **f**) TiO_2 (100 μg/mL) exposure. Scales are 500 μm. (**g**–**i**) Confocal image of cardiomyocytes on nanofiber, stained for nuclei (blue) and α-actinin (gray). Scales are 100 μm (for the top panels) and 20 μm (for the bottom panels). The bottom panels are the zoom-in images from the red dots of the top panels. (**j**) Orientational order parameter (OOP) analysis of cardiomyocytes after TiO_2 exposure. For statistical comparison with respect to control, $^{**}p < 0.05$, $n = 7$ for control (0 μg/mL) and TiO_2 (100 μg/mL) and $n = 6$ for TiO_2 (10 μg/mL)

a synchronized contraction of cardiomyocytes was also observed. However, the higher TiO_2 dose (100 μg/mL) caused a non-synchronous calcium transient (Fig. 6e, f; see ESM Movie 6) in line with the decreased contractility recorded using our MPS-based contractility assay (Figs. 4 and 5). The cardiac MPS samples exposed to cytotoxic Ag nanoparticles (50 μg/mL), as our positive control, consistently resulted in an impaired calcium transient propagation (see ESM Figs. S8a and S8b).

From our findings, we hypothesize that the higher dose exposure of TiO_2 nanoparticles can disrupt the sarcomere architecture, which correlates to the decreased contractile function observed in the cardiac MPS. To test this premise, we performed structural analysis of our cardiac tissue samples by immunostaining against sarcomeric α-actinin. Cardiomyocytes, without the nanoparticle exposure, formed an anisotropic tissue along the alignment of the nanofiber layers and revealed a perpendicular z-line registration (Fig. 6g) that plays a vital role in effective pump function. Cardiomyocytes with a low dose of TiO_2 nanoparticles still showed a similar organization of z-lines (Fig. 6h). However, the exposure to a high dose of TiO_2 or silver nanoparticles caused disruption of the sarcomeric z-line architecture (Fig. 6i; see ESM Fig. S8c). In order to quantify the sarcomere architecture, the OOP of sarcomeres at different ENM exposure conditions was calculated (Fig. 6j). There was no significant difference between control and low-dose TiO_2 (10 μg/mL) exposure samples. However, the OOP value of high-dose TiO_2 (100 μg/mL) exposure samples was significantly decreased with respect to the non-exposed control.

Even though we showed promising results using the fibrous MPS for screening the toxicity of ENMs, it should be noted that

there are still some technical limitations for these current devices. This system only includes one cell type (cardiomyocytes) as a proof-of-concept. However, heart or other organs are composed of multiple cell types and interconnected to other organs to function efficiently at the macroscopic level. To address this issue, future studies may include multicellular MPS to represent the complexity of native organs. Likewise, our systems can be integrated with multiple organs in one MPS to predict the toxicological impacts of ENMs by considering organ cross-talk and different ENM biodistribution routes. Beyond contractility, chronic "on-chip" measurement of action potentials using a high-throughput instrumented device with 3D scaffolds such as this would also be beneficial for future toxicology studies.

Altogether, our data demonstrated that the low-dose exposure of TiO_2 nanoparticles (10 μg/mL) does not significantly affect the structure and function of in vitro cardiomyocyte tissue samples within the time range of our ENM exposure studies. However, the high-dose exposure of TiO_2 nanoparticles (100 μg/mL) demonstrated impaired contractile function and damaged tissue structure after only 48 h of exposure. The dose-dependent cardiac effects of TiO_2 nanoparticles are in accordance with previously published work [51]. In addition to previously reported tissue damage, we also observed a decrease in sarcomere organization and interruptions in the propagation of calcium signaling, suggesting an underlying cause for functional tissue damage. This shows that the measurements of contractile function derived from the fiber-coated MPS presented herein, provided consistent insights with conventional cytotoxic and structural analyses of tissue impairment due to ENM exposure. Overall, these consistent observations validate the capability of our 3D fiber-coated MPS to be used as an in vitro analytical platform to assess the toxicological effects of ENMs to cardiac function at multiple time points.

Conclusions

In this study, we present a biomimetic platform that can be used as an in vitro analytical assay to determine the effects of different nanoparticles on cardiac tissue contractility. The engineered mussel-inspired nanofiber, which is comprised of PCL and PDA units, resulted in highly aligned constructs that provided a topographical cue for the consistent formation of anisotropic cardiac tissues across multiple samples. Moreover, the nanofiber facilitated cellular adhesion and ECM protein coating due to their bioadhesive property. Cardiomyocytes grown on the nanofiber scaffolds developed into mature and functional tissues, as confirmed by previously reported metrics. Finally, the fiber-coated cardiac microphysiological devices were developed and cultured with cardiomyocytes for the contractility assay and toxicity studies. The effects of direct ENM exposure were tested using our MPS device platform, which provided insights and established trends in the measured contractile behavior of cardiac tissues at different exposure conditions that were consistent with the disruption of normal sarcomere alignment in tissues and calcium signaling observed using conventional assays. In principle, the instrumented version of our 3D fiber-coated MPS enables a non-invasive method towards higher-throughput toxicological studies. Therefore, these findings demonstrate the capability of our 3D nanofibrous MPS platform not only to recapitulate the 3D native structure of the myocardium in vitro but also to serve as a reliable platform to study the cardiotoxic effects of engineered nanomaterials.

Acknowledgements The content is solely the responsibility of the authors and does not necessarily represent the official views of the National Institutes of Health. The engineered nanomaterials used in the research presented in this publication have been procured or synthesized and characterized by the Engineered Nanomaterials Resource and Coordination Core (ERCC) at the Center for Nanotechnology and Nanotoxicology at Harvard School of Public Health, part of the NIEHS/NHIR consortium. The authors also acknowledge the graphic works provided by Michael Rosnach. The authors also thank Dr. Patrick Campbell for providing information about the guidelines followed for animal experiments.

Funding information This work was supported by the Wyss Institute for Biologically Inspired Engineering at Harvard University. For the development and characterization of 3D nanofibrous MPS platform, this research was performed in part at the Harvard University Materials Research Science and Engineering Center (MRSEC) under NSF Award No. DMR-1420570 and the Harvard Center for Nanoscale Systems (CNS), which is a member of the National Nanotechnology Infrastructure Network (NNIN) under NSF Award No. 1541959. Research reported in this publication was supported by National Institute of Environmental Health Sciences of the National Institutes of Health under Award Number (NIH grant number U01ES027272) as part of the Nanotechnology Health Implications Research (NHIR) Consortium.

Compliance with ethical standards

Conflict of interest The authors declare that they have no conflict of interest.

Research involving human participants and/or animals The Faculty of Arts and Sciences (FAS) of Harvard University maintains an Institutional Animal Care and Use Committee (IACUC) as required by the Public Health Service (PHS) Policy on Humane Care and Use of Laboratory Animals. All protocols for animal experiments done in this study were approved by IACUC at Harvard University. All animals were appropriately housed prior to use. On arrival to our animal facility, neonatal rat pups used in the study and their dams were housed in clean, ventilated microisolator cages in a climate-controlled, automatic light cycle-equipped room with dam having free access to food and fresh water. All research personnel handling animals were appropriately qualified and trained by Harvard's Office of Animal Resources under the direction of the Attending Veterinarian. Our euthanasia method for the pups is consistent with the recommendations of the 2013 American Veterinary Medical Association (AVMA) Guidelines on Euthanasia for rodents. All rats used in this study were cared for and used in a manner that complies with the US Government Principles for the Utilization and Care of Vertebrate Animals Used in Testing, Research, and Training [63]; the Guide for the Care and Use of Laboratory Animals [64]; and the Animal Welfare Act/Regulations [65].

References

1. Walser T, Limbach LK, Brogioli R, Erismann E, Flamigni L, Hattendorf B, et al. Persistence of engineered nanoparticles in a municipal solid-waste incineration plant. Nat Nanotechnol. 2012;7(8):520.
2. Simeonova PP, Erdely A. Engineered nanoparticle respiratory exposure and potential risks for cardiovascular toxicity: predictive tests and biomarkers. Inhal Toxicol. 2009;21(sup1):68–73.
3. Yokel RA, MacPhail RC. Engineered nanomaterials: exposures, hazards, and risk prevention. J Occup Med Toxicol. 2011;6(1):7.
4. Gwinn MR, Vallyathan V. Nanoparticles: health effects—pros and cons. Environ Health Perspect. 2006;114(12):1818.
5. Stampfl A, Maier M, Radykewicz R, Reitmeir P, Göttlicher M, Niessner R. Langendorff heart: a model system to study cardiovascular effects of engineered nanoparticles. ACS Nano. 2011;5(7):5345–53.
6. Lin C-X, Yang S-Y, Gu J-L, Meng J, Xu H-Y, Cao J-M. The acute toxic effects of silver nanoparticles on myocardial transmembrane potential, I Na and I K1 channels and heart rhythm in mice. Nanotoxicology. 2017;11(6):827–37.
7. Mueller NC, Nowack B. Exposure modeling of engineered nanoparticles in the environment. Environ Sci Technol. 2008;42(12):4447–53.
8. Sun H, Xia M, Austin CP, Huang R. Paradigm shift in toxicity testing and modeling. AAPS J. 2012;14(3):473–80.
9. Grosberg A, Alford PW, McCain ML, Parker KK. Ensembles of engineered cardiac tissues for physiological and pharmacological study: heart on a chip. Lab Chip. 2011;11(24):4165–73.
10. Grosberg A, Nesmith AP, Goss JA, Brigham MD, McCain ML, Parker KK. Muscle on a chip: in vitro contractility assays for smooth and striated muscle. J Pharmacol Toxicol Methods. 2012;65(3):126–35.
11. Shim J, Grosberg A, Nawroth JC, Parker KK, Bertoldi K. Modeling of cardiac muscle thin films: pre-stretch, passive and active behavior. J Biomech. 2012;45(5):832–41.
12. McCain ML, Agarwal A, Nesmith HW, Nesmith AP, Parker KK. Micromolded gelatin hydrogels for extended culture of engineered cardiac tissues. Biomaterials. 2014;35(21):5462–71.
13. Lind JU, Busbee TA, Valentine AD, Pasqualini FS, Yuan H, Yadid M, et al. Instrumented cardiac microphysiological devices via multimaterial three-dimensional printing. Nat Mater. 2017;16(3):303.
14. Lind JU, Yadid M, Perkins I, O'Connor BB, Eweje F, Chantre CO, et al. Cardiac microphysiological devices with flexible thin-film sensors for higher-throughput drug screening. Lab Chip. 2017;17(21):3692–703.
15. Feinberg AW, Feigel A, Shevkoplyas SS, Sheehy S, Whitesides GM, Parker KK. Muscular thin films for building actuators and powering devices. Science. 2007;317(5843):1366–70.
16. Agarwal A, Goss JA, Cho A, McCain ML, Parker KK. Microfluidic heart on a chip for higher throughput pharmacological studies. Lab Chip. 2013;13(18):3599–608.
17. McCain ML, Sheehy SP, Grosberg A, Goss JA, Parker KK. Recapitulating maladaptive, multiscale remodeling of failing myocardium on a chip. Proc Natl Acad Sci. 2013;110(24):9770–5.
18. Nesmith AP, Agarwal A, McCain ML, Parker KK. Human airway musculature on a chip: an in vitro model of allergic asthmatic bronchoconstriction and bronchodilation. Lab Chip. 2014;14(20):3925–36.
19. Wang G, McCain ML, Yang L, He A, Pasqualini FS, Agarwal A, et al. Modeling the mitochondrial cardiomyopathy of Barth syndrome with induced pluripotent stem cell and heart-on-chip technologies. Nat Med. 2014;20(6):616.
20. Pham QP, Sharma U, Mikos AG. Electrospinning of polymeric nanofibers for tissue engineering applications: a review. Tissue Eng. 2006;12(5):1197–211.
21. Badrossamay MR, McIlwee HA, Goss JA, Parker KK. Nanofiber assembly by rotary jet-spinning. Nano Lett. 2010;10(6):2257–61.
22. Badrossamay MR, Balachandran K, Capulli AK, Golecki HM, Agarwal A, Goss JA, et al. Engineering hybrid polymer-protein super-aligned nanofibers via rotary jet spinning. Biomaterials. 2014;35(10):3188–97.
23. Deravi LF, Sinatra NR, Chantre CO, Nesmith AP, Yuan H, Deravi SK, et al. Design and fabrication of fibrous nanomaterials using pull spinning. Macromol Mater Eng. 2017;302(3):1600404.
24. Liu Y, Ai K, Lu L. Polydopamine and its derivative materials: synthesis and promising applications in energy, environmental, and biomedical fields. Chem Rev. 2014;114(9):5057–115.
25. Lin Q, Gourdon D, Sun C, Holten-Andersen N, Anderson TH, Waite JH, et al. Adhesion mechanisms of the mussel foot proteins mfp-1 and mfp-3. Proc Natl Acad Sci. 2007;104(10):3782–6.
26. Lee H, Rho J, Messersmith PB. Facile conjugation of biomolecules onto surfaces via mussel adhesive protein inspired coatings. Adv Mater. 2009;21(4):431–4.
27. Chuah YJ, Koh YT, Lim K, Menon NV, Wu Y, Kang Y. Simple surface engineering of polydimethylsiloxane with polydopamine for stabilized mesenchymal stem cell adhesion and multipotency. Sci Rep. 2015;5:18162.
28. Ku SH, Park CB. Human endothelial cell growth on mussel-inspired nanofiber scaffold for vascular tissue engineering. Biomaterials. 2010;31(36):9431–7.
29. Dhand C, Barathi VA, Ong ST, Venkatesh M, Harini S, Dwivedi N, et al. Latent oxidative polymerization of catecholamines as potential cross-linkers for biocompatible and multifunctional biopolymer scaffolds. ACS Appl Mater Interfaces. 2016;8(47):32266–81.
30. Choi W, Lee S, Kim SH, Jang JH. Polydopamine inter-fiber networks: new strategy for producing rigid, sticky, 3D fluffy electrospun fibrous polycaprolactone sponges. Macromol Biosci. 2016;16(6):824–35.
31. Della Vecchia NF, Luchini A, Napolitano A, D'Errico G, Vitiello G, Szekely N, et al. Tris buffer modulates polydopamine growth, aggregation, and paramagnetic properties. Langmuir. 2014;30(32):9811–8.
32. Klosterman L, Ahmad Z, Viswanathan V, Bettinger CJ. Synthesis and measurement of cohesive mechanics in polydopamine nanomembranes. Adv Mater Interfaces. 2017;4(10):1700041.
33. Patel K, Singh N, Yadav J, Nayak JM, Sahoo SK, Lata J, et al. Polydopamine films changes their physiochemical and antimicrobial properties with change in reaction conditions. Phys Chem Chem Phys. 2018;20(8):5744–55.
34. Hotaling NA, Bharti K, Kriel H, Simon CG. DiameterJ: a validated open source nanofiber diameter measurement tool. Biomaterials. 2015;61:327–38.
35. Chan FK-M, Moriwaki K, De Rosa MJ. Detection of necrosis by release of lactate dehydrogenase activity. In: Snow A, Lenardo M, editors. Immune homeostasis. Methods in molecular biology (methods and protocols), vol. 979. Totowa: Humana Press; 2013. p. 65–70.
36. Ahn S, Chantre CO, Gannon AR, Lind JU, Campbell PH, Grevesse T, et al. Soy protein/cellulose nanofiber scaffolds mimicking skin extracellular matrix for enhanced wound healing. Adv Healthcare Mater. 2018:1701175. https://doi.org/10.1002/adhm.201701175.
37. Sheehy SP, Pasqualini F, Grosberg A, Park SJ, Aratyn-Schaus Y, Parker KK. Quality metrics for stem cell-derived cardiac myocytes. Stem Cell Rep. 2014;2(3):282–94.
38. Pasqualini FS, Sheehy SP, Agarwal A, Aratyn-Schaus Y, Parker KK. Structural phenotyping of stem cell-derived cardiomyocytes. Stem Cell Rep. 2015;4(3):340–7.

39. Tran QH, Le A-T. Silver nanoparticles: synthesis, properties, toxicology, applications and perspectives. Adv Nat Sci Nanosci Nanotechnol. 2013;4(3):033001.
40. Lee KJ, Jun BH, Kim TH, Joung J. Direct synthesis and inkjetting of silver nanocrystals toward printed electronics. Nanotechnology. 2006;17(9):2424.
41. Beltran-Huarac J, Zhang Z, Pyrgiotakis G, DeLoid G, Vaze N, Demokritou P. Development of reference metal and metal oxide engineered nanomaterials for nanotoxicology research using high throughput and precision flame spray synthesis approaches. NanoImpact. 2018;10:26–37.
42. DeLoid GM, Cohen JM, Pyrgiotakis G, Demokritou P. Preparation, characterization, and in vitro dosimetry of dispersed, engineered nanomaterials. Nat Protoc. 2017;12(2):355.
43. DeLoid GM, Cohen JM, Pyrgiotakis G, Pirela SV, Pal A, Liu J, et al. Advanced computational modeling for in vitro nanomaterial dosimetry. Part Fibre Toxicol. 2015;12(1):32.
44. DeLoid G, Cohen JM, Darrah T, Derk R, Rojanasakul L, Pyrgiotakis G, et al. Estimating the effective density of engineered nanomaterials for in vitro dosimetry. Nat Commun. 2014;5:3514.
45. Taurozzi JS, Hackley VA, Wiesner MR. Ultrasonic dispersion of nanoparticles for environmental, health and safety assessment—issues and recommendations. Nanotoxicology. 2011;5(4):711–29.
46. Dvir T, Timko BP, Brigham MD, Naik SR, Karajanagi SS, Levy O, et al. Nanowired three-dimensional cardiac patches. Nat Nanotechnol. 2011;6(11):720.
47. Liebscher J, Mrówczyński R, Scheidt HA, Filip C, Hădade ND, Turcu R, et al. Structure of polydopamine: a never-ending story? Langmuir. 2013;29(33):10539–48.
48. Xie J, Michael PL, Zhong S, Ma B, MacEwan MR, Lim CT. Mussel inspired protein-mediated surface modification to electrospun fibers and their potential biomedical applications. J Biomed Mater Res A. 2012;100((4):929–38.
49. Zangmeister RA, Morris TA, Tarlov MJ. Characterization of polydopamine thin films deposited at short times by autoxidation of dopamine. Langmuir. 2013;29(27):8619–28.
50. Boudreau-Béland J, Duverger JE, Petitjean E, Maguy A, Ledoux J, Comtois P. Spatiotemporal stability of neonatal rat cardiomyocyte monolayers spontaneous activity is dependent on the culture substrate. PLoS One. 2015;10(6):e0127977.
51. Jawad H, Boccaccini AR, Ali NN, Harding SE. Assessment of cellular toxicity of TiO_2 nanoparticles for cardiac tissue engineering applications. Nanotoxicology. 2011;5(3):372–80.
52. Mallik A, Bryan S, Puukila S, Chen A, Khaper N. Efficacy of Pt-modified TiO_2 nanoparticles in cardiac cells. Exp Clin Cardiol. 2011;16(1):6.
53. Schwerdt A, Zintchenko A, Concia M, Roesen N, Fisher K, Lindner LH, et al. Hyperthermia-induced targeting of thermosensitive gene carriers to tumors. Hum Gene Ther. 2008;19(11):1283–92.
54. Bostan HB, Rezaee R, Valokala MG, Tsarouhas K, Golokhvast K, Tsatsakis AM, et al. Cardiotoxicity of nano-particles. Life Sci. 2016;165:91–9.
55. Duan Y, Liu H, Zhao J, Liu C, Li Z, Yan J, et al. The effects of nano-anatase TiO_2 on the activation of lactate dehydrogenase from rat heart. Biol Trace Elem Res. 2009;130(2):162–71.
56. Sheng L, Wang X, Sang X, Ze Y, Zhao X, Liu D, et al. Cardiac oxidative damage in mice following exposure to nanoparticulate titanium dioxide. J Biomed Mater Res A. 2013;101(11):3238–46.
57. Savi M, Rossi S, Bocchi L, Gennaccaro L, Cacciani F, Perotti A, et al. Titanium dioxide nanoparticles promote arrhythmias via a direct interaction with rat cardiac tissue. Part Fibre Toxicol. 2014;11(1):63.
58. Chen J, Dong X, Xin Y, Zhao M. Effects of titanium dioxide nanoparticles on growth and some histological parameters of zebrafish (Danio rerio) after a long-term exposure. Aquat Toxicol. 2011;101(3-4):493–9.
59. Carlson C, Hussain SM, Schrand AM, Braydich-Stolle LK, Hess KL, Jones RL, et al. Unique cellular interaction of silver nanoparticles: size-dependent generation of reactive oxygen species. J Phys Chem B. 2008;112(43):13608–19.
60. AshaRani P, Low Kah Mun G, Hande MP, Valiyaveettil S. Cytotoxicity and genotoxicity of silver nanoparticles in human cells. ACS Nano. 2008;3(2):279–90.
61. Han X, Gelein R, Corson N, Wade-Mercer P, Jiang J, Biswas P, et al. Validation of an LDH assay for assessing nanoparticle toxicity. Toxicology. 2011;287(1-3):99–104.
62. Altunbek M, Culha M. Influence of plasmonic nanoparticles on the performance of colorimetric cell viability assays. Plasmonics. 2017;12(6):1749–60.
63. Interagency Research Animal Committee. US government principles for the utilization and care of vertebrate animals used in testing, research and training. 2010;13. https://grants.nih.gov/grants/olaw/references/phspol.htm#USGovPrinciples. Accessed Dec 2010.
64. National Research Council. Guide for the care and use of laboratory animals. Washington, D.C.: National Academies Press; 2010.
65. US Department of Health and Human Services. Code of federal regulations: title 9: part 1: chapter 1: subchapter A: animal welfare. 2009;1.